International Journal of Solids and Structures 113–114 (2017) 218–229

Contents lists available at ScienceDirect

International Journal of Solids and Structures

journal homepage: www.elsevier.com/locate/ijsolstr

Homogenization of porous piezoelectric materials

Germán Martínez-Ayuso[a,*], Michael I. Friswell[a], Sondipon Adhikari[a], Hamed Haddad Khodaparast[a], Harald Berger[b]

[a] Swansea University, Bay Campus Fabian Way, Crymlyn Burrows, Swansea SA1 8EN, Wales, United Kingdom
[b] Institute of Mechanics, Faculty of Mechanical Engineering, University of Magdeburg, Universitaetsplatz 2, D-39106 Magdeburg, Germany

ARTICLE INFO

Article history:
Received 19 February 2016
Revised 26 February 2017
Available online 16 March 2017

Keywords:
Piezoelectricity
Porous
Homogenization
Numerical
Mori-Tanaka
Finite element method

ABSTRACT

This paper presents a homogenization study of porous piezoelectric materials through analytical and numerical analysis. Using two of the most well-known analytical methods for theoretical homogenization, the Mori–Tanaka and self-consistent schemes, the full set of material properties are obtained. These results are compared to two different theoretical bounds, the Halpin–Tsai and Hashin–Sthrikman bounds. A numerical model of a representative volume element is then developed using finite element analysis for different percentages of inclusions. Finally, the analytical and numerical results are compared and discussed; a good agreement between the analytical and numerical methods is shown.

1. Introduction

The piezoelectrical effect is the capacity exhibited by some materials to convert strain to electrical energy and electrical energy to strain. Piezoelectric materials have received significant attention due to their use in devices such as sensors, to measure strain or voltage, actuators and energy harvesters (Kara et al., 2003; Newnham, 1986). Many authors have worked on the use of the piezoelectric materials for energy harvesters. Ertuk and Inman (2008; 2009; 2011) studied the piezoelectric cantilever bimorph beam for energy harvesting, from theoretical to experimental cases. Sodano extensively reviewed the applications of piezoelectric materials for energy harvesting (Anton and Sodano, 2007; Sodano et al., 2004; 2005). Friswell and Adhikari explored the possibilities of piezoelectric devices to harvest energy under non-linear vibration (Friswell et al., 2012) and broadband excitation (Adhikari et al., 2009). The piezoelectric material properties, from a general point of view, are defined by two parameters, the electromechanical coupling and the capacitance, which depend on the piezoelectric coefficients and the geometry. The coupling measures the amount of mechanical energy the material can convert to electrical energy and the capacitance measures the losses in the generating of the electrical field which will remain confined in the material. These coefficients depend on the geometry and material properties. Looking at the material impact on these coefficients, the capacitance depends on the permittivity of the material as well as other non-material related parameters such as electrode area and thickness. The coupling is proportional to the piezoelectric coefficients (Erturk and Inman, 2011). Clearly it is desirable to have high coupling and low capacitance, in order to maximize the energy output. Material science has discovered new ceramics PZT materials with higher coupling effects which mean higher energy generated. The use of composite materials can improve the characteristics of bulk materials. Different applications, for example naval or aerospace, require high values of parameters such as stiffness, strength or piezoelectrical coupling. Unfortunately, piezoelectric ceramic materials are quite brittle, and do not support the high deformation which is desirable for the high strains required to generate high voltages for energy harvesting or sensing (Vijaya, 2012). Also, the piezoelectric coefficients are an intrinsic property of the material and so there is limited potential to modify them without using composite science, i.e. mixing the piezoelectric material with other piezo or non-piezo in order to increase or decrease the piezoelectric coefficients. One solution to improve these elastic properties is to mix the brittle PZT with more flexible materials like polymers, so that the composite resultant material has better general properties, depending on the properties of the material added to the piezoelectric phase, such as its structure, electromechanical properties and percentage added. For these reasons, most attention has been given to composites made of piezoelectric materials and polymers. In an early work about analytical piezoelectric composites, Newnham (1986) explored the

* Corresponding author.
E-mail addresses: 841238@swansea.ac.uk (G. Martínez-Ayuso), m.i.friswell@swansea.ac.uk (M.I. Friswell), s.adhikari@swansea.ac.uk (S. Adhikari), h.haddadkhodaparast@swansea.ac.uk (H.H. Khodaparast), harald.berger@ovgu.de (H. Berger).

http://dx.doi.org/10.1016/j.ijsolstr.2017.03.003
0020-7683/

properties, the connectivity patterns, and the symmetry of the composite. He realised the relation between the connectivity and the field and force concentration. Gururaja et al. (1985) studied the use of piezoelectric composites as transducers. Different tests were performed to measure the resonance modes also considering the temperature effect. Beeby et al. (2006) reviewed applications of piezoelectricity in microsystem applications for energy harvesting. Cook-Chennault et al. (2008) investigated the use of the piezoelectric devices to supply energy to micro-electro-mechanical systems (MEMS). For the correct design of piezoelectric composite devices it is necessary to have some a priori estimate of the percentage of each phase and the resulting parameters (elastic, piezoelectric and dielectric coefficients) to control the piezoelectric coefficients and their stress-charge counterpart. These estimates can be obtained from analytical theories, numerical models (FEM models) and/or characterization experiments.

For the analytical approach, different authors have worked on piezoelectric materials homogenization. Nemat-Nasser and Hori (1993) considered the homogenization of heterogeneous materials. In this book, an analytical study of different heterogeneous composites was given, from composites which contains inhomogeneities to those which have micro-cracks. Dunn and Taya (1993a) extended the Mori–Tanaka method, one of the most reliable analytical homogenization methods, to include the electrical coupling of the piezoelectric materials. Also, they calculated the corresponding Eshelby tensor (Dunn and Taya, 1993a) which is required to calculate analytically the relation between the strain inside the inclusion and the macro-strain (Eshelby, 1957) and hence the electro-mechanical matrix of the corresponding homogenized material. One approach to increase the efficiency of piezoelectric devices is to increase the piezoelectrical coupling to harvest more energy. This approach is followed when PZT-polymer composites are used. The other approach is to decrease the capacitance, through modifying the piezoelectrical and dielectric coefficients by adding a new phase to the composite material. In this sense, the porous piezoelectric materials represent a good alternative to the traditional PZT-polymer composites. Little emphasis has been given to porous piezoelectrics, although they exhibit good piezoelectric properties and low capacitance (Kara et al., 2003). Li et al. (2003) characterized porous piezoelectric material from experimental results. Roncari et al. (2001) elaborated a comprehensive review of the different methods to prepare porous piezoelectric ceramics. Bowen et al. (2004) reviewed the experimental figures of merit for different fabrication processes, such as poly(methyl methacrylate) (PMMA), self-raising and burn out polymer spheres process (BurPS). Roscow et al. (2015) applied piezoelectric porous material to energy harvesting using piezoelectricity, pyroelectricity and ferroelectricity properties. Until now, few studies has been performed on the analytical homogenization of porous piezoelectric materials. Dunn and Taya (1993b) used the Mori–Tanaka approach to evaluate the properties of porous PZT. In addition to the analytical models, homogenization can be performed by a numerical approach using FE techniques. Different authors have highlighted the validity of such techniques for different fields such as elasticity (Miehe et al., 2002; Geers et al., 2010; Kouznetsova et al., 2004; Terada et al., 2000), plasticity (Miehe et al., 1999; Fish et al., 1997), non-linearities (Geers et al., 2001; Feyel, 2003), complex microstructures (Moës et al., 2003; Terada et al., 2000), etc... Other authors have studied the distribution of the inclusions using statistical approaches to account for randomness in the location of the inclusions (Balzani et al., 2014; Schröder et al., 2011). Kar-Gupta and Venkatesh (2007) analysed through a finite element model the influence of the porosity percentage and the orientation of the inclusion on the effective parameters.

A new approach to the porous piezoelectrical material homogenization is proposed and a comparison between theoretical models and numerical results is given. A theoretical analysis of the porous piezoelectric material is proposed using mean-field homogenization methods, such as the self-consistent scheme and the Mori–Tanaka approach, which are used to determine the homogenized material properties. Also, two bounds are given to contrast the different limit values. These results are compared to a finite element model, which represents the most favourable case. The most favourable case is when the distribution of inclusions is spatially homogeneous and the inclusion shape is a perfect sphere which gives a perfectly transverse isotropic material. The influence of the different percentages of inclusions is studied for both approaches, analytical and numerical.

The present paper has 6 sections. An introduction and justification of this work is made in the first section. The mathematical notation which will be followed in the paper, is defined in the second part. The third section, gives a brief review of the techniques for analytical homogenization, such as the Mori–Tanaka method and self-consistent methods. Also, we compare these methods with common theoretical bounds, namely the Halpin–Tsai bounds and Hashin–Sthrikman bounds. In the fourth section finite element modelling of the representative volume element (RVE), and a verification of the analytical theories, is performed. The characteristics of the model and the procedure of verification via the material parameters of the homogenised material are also described. The results of the analytical theories and finite element models are summarized in the fifth section, together with a discussion of the implications of porosity on the energy harvesting performance of piezoelectric materials. Finally, conclusions are given at the end of the paper.

2. Mathematical preliminaries and notation

In piezoelectricity the governing equations for a linear static case without body charge or forces are given by

$$\sigma_{ij} = C_{ijmn}\,\epsilon_{mn} - e_{nij}\,E_n \quad \text{and}$$
$$D_i = e_{imn}\,\epsilon_{mn} - k_{in}\,E_n \tag{1}$$

In these equations, the independent variables are the elastic strain ϵ_{mn} and the electric field E_n. These variables are related to the stress σ_{ij} and the electric displacement D_i by C_{ijmn}, e_{nij} and k_{in} which are the elastic constitutive matrix (measured in a constant electric field), the piezoelectric coefficients matrix (measured at a constant strain or electric field) and the dielectric constant matrix (measured at a constant strain), respectively. Due to the multiphysics nature of the piezoelectric effect, we need to use a consistent notation which accounts for this coupled nature. The notation used here is a modification of the Einstein notation (repeated subscripts are summed over the range 1–3) that was developed by Barnett and Lothe (1975) and by Dunn and Taya (1993c). This notation is identical to that of Einstein with the exception that lower case subscripts have the range 1–3 while upper-case subscripts have the range 1–4, and repeated upper-case subscripts are summed over 1–4. A comma in the sub-index denotes partial differentiation. When the piezoelectric effect is included, Z_{Mn} is the elastic strain and electric field coupled vector, and is expressed as

$$Z_{Mn} = \begin{cases} \epsilon_{mn}, & M = 1, 2, 3, \\ -E_n, & M = 4, \end{cases} \tag{2}$$

Similarly, we obtain the stress and electric displacement coupled vector which is defined as

$$\Sigma_{iJ} = \begin{cases} \sigma_{ij}, & J = 1, 2, 3, \\ D_i, & J = 4, \end{cases} \tag{3}$$

The electroelastic material matrix can then be represented as

$$E_{iJMn} = \begin{cases} C_{ijmn} & J, M = 1, 2, 3, \\ e_{nij} & J = 1, 2, 3; M = 4, \\ e_{imn} & J = 4; M = 1, 2, 3 \\ k_{in} & J, M = 4, \end{cases} \tag{4}$$

The inverse of the electro-elastic material matrix is the compliance electro-elastic matrix F_{AbiJ}. The properties of these matrices are derived from their constitutive elements C_{ijmn}, e_{nij} and k_{in}, which means these matrices are symmetric. With this notation we obtain the constitutive laws of the piezoelectric materials in matrix form as

$$\Sigma_{iJ} = E_{iJMn} Z_{Mn} \tag{5}$$

and $$Z_{Ab} = F_{AbiJ} \Sigma_{iJ} \tag{6}$$

It is important to note that Z_{Mn}, U_M, Σ_{iJ}, E_{iJMn}, and F_{AbiJ} are not tensors (Dunn and Taya, 1993a). Hence each individual tensor must be transformed by the well known laws of tensor transformation to write corresponding equations in an alternate coordinate system.

Equivalently, Eq. (5) can be written in condensed form (Dunn and Taya, 1993b) as

$$\begin{pmatrix} \sigma_{11} \\ \sigma_{22} \\ \sigma_{33} \\ \sigma_{23} \\ \sigma_{13} \\ \sigma_{12} \\ D_1 \\ D_2 \\ D_3 \end{pmatrix} = \left(\begin{array}{cccccc|ccc} C_{11} & C_{12} & C_{13} & C_{14} & C_{15} & C_{16} & -e_{11} & -e_{12} & -e_{13} \\ C_{21} & C_{22} & C_{23} & C_{24} & C_{25} & C_{26} & -e_{21} & -e_{22} & -e_{23} \\ C_{31} & C_{32} & C_{33} & C_{34} & C_{35} & C_{36} & -e_{31} & -e_{32} & -e_{33} \\ C_{41} & C_{42} & C_{43} & C_{44} & C_{45} & C_{46} & -e_{41} & -e_{42} & -e_{43} \\ C_{51} & C_{52} & C_{53} & C_{54} & C_{55} & C_{56} & -e_{51} & -e_{52} & -e_{53} \\ C_{61} & C_{62} & C_{63} & C_{64} & C_{65} & C_{66} & -e_{61} & -e_{62} & -e_{63} \\ \hline e_{11} & e_{12} & e_{13} & e_{14} & e_{15} & e_{16} & k_{11} & k_{12} & k_{13} \\ e_{21} & e_{22} & e_{23} & e_{24} & e_{25} & e_{26} & k_{21} & k_{22} & k_{23} \\ e_{31} & e_{32} & e_{33} & e_{34} & e_{35} & e_{36} & k_{31} & k_{32} & k_{33} \end{array}\right) \cdot \begin{pmatrix} \epsilon_{11} \\ \epsilon_{22} \\ \epsilon_{33} \\ \epsilon_{23} \\ \epsilon_{13} \\ \epsilon_{12} \\ E_1 \\ E_2 \\ E_3 \end{pmatrix} \tag{7}$$

The different materials considered will be specified by the superindex, being the value "*I*" for the inclusion parameters and "*M*" for the matrix parameters. When there is more than one inclusion phase, the phase inclusion considered is denoted by "*r*". We also notice that all the different parameters have their equivalent at the macro-scale and they are denoted with an over bar, for example, $\overline{\boldsymbol{\Sigma}}$ or $\overline{\boldsymbol{Z}}$.

3. Analytical homogenization approach

3.1. Introduction

Since linear behaviour is assumed throughout the composite, it is logical to assume the response of the composite material is a superposition of the response of the different phases averaged in some way. The composite response is determined by the homogenized composite properties called "effective properties" or "macro-properties". These macro-properties, $\overline{\boldsymbol{\Sigma}}$ and $\overline{\boldsymbol{Z}}$, also have to be consistent with the energy conservation principle, that means the virtual work, *W*, on a given material volume, *V*, at the macro-scale must be equal to the virtual work at the micro-scale. Thus

$$\delta \overline{W} = \frac{1}{V} \int_V \delta W \, dV \tag{8}$$

The Hill-Mandel condition is fulfilled when we apply linear displacements, uniform tractions, mixed boundary conditions or periodic boundary conditions on *dV* (Nemat-Nasser and Hori, 1993; Nemat-Nasser et al., 1993). The choice of boundary conditions is discussed in Section 4.2. When we apply one of these boundary conditions, the variables such as strain, stress, electrical displacement and electrical field in a finite volume *V* are equal to the macro equivalent variable, namely macro strain, macro stress, macro electrical displacement, and macro electrical field.

From Eq. (8), an averaging process of the different parameters from the microlevel to the macroscopic level gives the relations

$$\overline{\boldsymbol{\Sigma}}^I = \frac{1}{V^I} \int_{V^I} \boldsymbol{\Sigma} \, dV \quad , \quad \overline{\boldsymbol{Z}}^M = \frac{1}{V^M} \int_{V^M} \boldsymbol{Z} \, dV \tag{9}$$

The Hill-Mandel conditions mean that the variations in strain, stress, electrical displacement and electrical fields at the micro-scale influence the macroscopic response only through its volumetric mean value. This is derived from the energy conservation principle. Also, gradients in strain, stress, electrical displacement and electrical field are not significant at the micro-scale, and so these gradients are assumed constant. This is derived from the linearity assumed at the beginning. All these assumptions shape the *Mean-Field Homogenization Theory* which is the basis of the analytical study developed in this paper.

From the assumptions made previously and Eq. (9), a simple volume averaged over a suitable cell, called a representative volume element (RVE), can estimate the overall properties (Dunn and Taya, 1993c; 1993b; Hill, 1963; Odegard, 2004). The chosen volume must be statistically representative of the material at the macroscale. The required RVE properties will be discussed more in depth in Section 4.1. Accordingly to these suppositions, the volume-averaged fields of the composite with *N* phases can be obtained using the averaged summations as

$$\overline{\boldsymbol{\Sigma}} = \sum_{r=1}^{N} c^r \boldsymbol{\Sigma}^r \quad \text{and}$$

$$\overline{\boldsymbol{Z}} = \sum_{r=1}^{N} c^r \boldsymbol{Z}^r \tag{10}$$

where c_r is the volume fraction of the phase *r*, the overbar denotes a volume-averaged quantity or macro-parameter and $r = 1$ is the matrix phase. The constitutive equation of each phase is given by Eq. (7).

Following this approach the constitutive equations for the composite can be expressed in term of the volume-averaged fields as

$$\overline{\boldsymbol{\Sigma}} = \overline{\boldsymbol{E}} \, \overline{\boldsymbol{Z}} \tag{11}$$

3.2. Eshelby solution

A composite material can be described as one or more well-defined phases inside a matrix made of other material different to those of the phases. These phases have a defined boundary with the matrix, so these phases have specific shapes (layers, fibers, spheres, ellipsoids, etc.). Depending on the geometry of the inclusions, the solution or procedure is different. The study of the analytical solution of an ellipsoidal inclusion inside a matrix was realised by Eshelby (1957). He considered that the matrix was infinite compared with the size of the inclusion. This assumption holds for non-high inclusion percentages; some authors reported the maximum percentage is about 50 percent (Dunn and Taya, 1993a; 1993b). Eshelby developed relations between the stress and

strain in the inclusion and the matrix through a concentration tensor called the "Eshelby Tensor". This tensor relates the constrained strain inside the inclusion with their eigenstrain (Eshelby, 1957). This solution, based on the linearity of the material behaviour, solves the Green's function for the elliptical shape. The solution has been extended by varying the dimensions of the ellipsoid axis, for fibers (one of the axis is infinite), spheres (all axis are equal) or cracks (one of the axis is zero) or for non-elliptical shapes such as arbitrary polygons or those characterized by the finite Laurent series (Klusemann et al., 2012; Zou et al., 2010). For an ellipsoidal inclusion in a homogeneous infinite matrix, the Eshelby Tensor is constant, due to the uniform relationship between the stress and strain fields. This relationship was demonstrated in Eshelby (1957) using a tensor D_{ijkl} which relates the displacement gradients to the stress inside the inclusion. The Eshelby tensor can be calculated using different approaches, such as calculating the electro-elastic Green's function or solving the integrals associated with the inclusion problem. Dunn and Taya extended this tensor to include piezoelectrical materials (Dunn and Taya, 1993a). Based on the previous works of Deeg (1980) , they obtained the four tensors necessary to define the elastic, piezoelectric and dielectric properties of an ellipsoidal inclusion embedded in an infinite matrix. One of these tensors is the piezoelectric equivalent tensor or simply the Eshelby tensor. In this paper, the Eshelby tensor is calculated by solving the inclusion integrals following the procedure described in Mikata (2000). To obtain the Eshelby tensor for a given material, only the nature of the matrix (isotropic, transverse isotropic, orthotropic, etc) and the shape of the inclusion are required, and this tensor changes depending on the geometry considered such as, fibre, sphere or ellipsoid. In our case, we consider a piezoelectric material matrix behaviour which is transverse isotropic and with spherical inclusions. The Eshelby tensor by itself cannot be used to homogenize a composite material, but it is the basis of the analytical homogeneization and is used in the most important theoretical approaches such as the Mori–Tanaka method and the self-consistent scheme (Klusemann and Svendsen, 2010).

3.3. Mori–Tanaka method

The Mori–Tanaka method (Mori and Tanaka, 1973) was developed for calculating the average internal stress in one matrix which contains precipitates with eigenstrains. Benveniste (1987) extended this approach to composite materials, considering anisotropic phases and ellipsoidal phases (Kurukuri and Eckardt, 2004). In this method each inclusion behaves as an isolated inclusion, embedded in an infinite matrix with properties $\boldsymbol{E^M}$ that is loaded remotely by an applied strain. Hence each inclusion is subjected to the averaged stress fields acting on it from all the other inclusions, through the superposition of stresses. The procedure of this method is detailed next. Firstly, an influence tensor has to be calculated for every phase r ($\boldsymbol{A}_0^{I,r}$). This concentration tensor is assumed to be equal to the relation between the strain in the inclusion with the strain in the matrix (Klusemann and Svendsen, 2010).

$$\boldsymbol{E}^{I,r} = \boldsymbol{A}_0^{I,r}\,\boldsymbol{E}^M \tag{12}$$

This concentration tensor is written in terms of the Eshelby tensor $\boldsymbol{S^*}$

$$\boldsymbol{A}_0^{I,r} = \left[\boldsymbol{I} + \boldsymbol{S^*}\left(\boldsymbol{E}^M\right)^{-1}\left(\boldsymbol{E}^{I,r} - \boldsymbol{E}^M\right)\right]^{-1} \tag{13}$$

Later, these concentration tensors will be averaged to obtain a general influence tensor ($\boldsymbol{A_{I(MT)}}$)

$$\boldsymbol{A}_{(MT)}^{I,r} = \left[c^{I,r}\boldsymbol{I} + c^M\left(\boldsymbol{A}_0^{I,r}\right)^{-1} + \sum_{j=1}^{N} c^{I,r}\boldsymbol{A}_0^{I,j}\left(\boldsymbol{A}_0^{I,r}\right)^{-1}\right]^{-1} \tag{14}$$

And finally we obtain the effective electro-elastic material tensor ($\boldsymbol{E^*}$) as

$$\boldsymbol{E}_{(MT)}^{*} = \boldsymbol{E}^M + \sum_{r=1} c^{I,r}\left(\boldsymbol{E}^{I,r} - \boldsymbol{E}^M\right)\boldsymbol{A}_{(MT)}^{I,r} \tag{15}$$

This method is considered also self-consistent since the inverse of the electromechanical matrix $\boldsymbol{E^*}$ is equal to the compliance electromechanical matrix $\boldsymbol{F^*}$.

3.4. Self-consistent method

The self-consistent method of Hershey (1954) and Kröner (1958) was originally proposed for aggregates of crystals and extended by Hill (1965) for application to composites. The self-consistent method (SCM) approximates the interaction between the phases by assuming that each phase is embedded in some equivalent medium with electroelastic properties $\boldsymbol{E^*}$, which represents the influence of all other inclusions (Mishnaevsky Jr, 2007). A priori, the value of $\boldsymbol{E^*}$ is unknown, so an iteration scheme has to be used. According to Norris (1985), the SCM has two groups, symmetric models where the phases are interchangeable and none of them are dominant, or asymmetric models were one phase is taken as a matrix phase, and the rest are all inclusions. Asymmetric models are preferred by Wu (1966) and Boucher (1974) although, for the sphere inclusion shape, both approaches lead to the same result. In general, the self-consistent method gives a sufficient prediction of the behaviour of poly-crystals but it is less accurate in the case of two-phase composites (Pierard et al., 2004). In the present work, a variant of the self-consistent method is used based on the Zouari approach (Zouari et al., 2008). The procedure relies on a progressive introduction of the inclusions in the matrix. For each step the behaviour of the homogenized medium is obtained by the self-consistent method and is used as the matrix of the following step. In the SCM, we account for the influence of each phase through an influence tensor, which is also related to the Eshelby tensor. One can obtain the influence tensor for each step N as

$$\boldsymbol{A}_{(N-1),(SCM)}^{r} = \left[\boldsymbol{I} + \boldsymbol{S^*}\left(\boldsymbol{E}_{(N-1)}^{*}\right)^{-1}\left(\boldsymbol{E}^{I,r} - \boldsymbol{E}_{(N-1)}^{*}\right)\right]^{-1} \tag{16}$$

The parameter $\boldsymbol{A}_{(N-1),(SCM)}^{r}$ is the concentration tensor for the self-consistent method (SCM) for the phase r in step $(N-1)$. This method gives the electromechanical properties $\boldsymbol{E_N^*}$ for the self-consistent scheme as

$$\boldsymbol{E}_{N,(SCM)}^{*} = \boldsymbol{E}^M + \sum_{r=1}^{N}\left(c_N^{I,r} - c_{(N-1)}^{I,r}\right)\left(\boldsymbol{E}^{I,r} - \boldsymbol{E}^M\right)\boldsymbol{A}_{(N-1),(SCM)}^{r} \tag{17}$$

The main difference between the self-consistent scheme and the Mori–Tanaka method is that Mori-Tanaka accounts for the effect of other inclusions through the concentration tensor, whereas the self-consistent method considers this effect using the effective properties of the embedded material inclusions as matrix properties.

3.5. Halpin–Tsai bounds

These bounds are one of the most popular approaches for composite homogenization. They are based upon the "self-consistent method" developed by Hill (1963) which Hermans (1967) employed to obtain a solution in terms of Hill's "reduced moduli". Later Halpin and Tsai reduced Hermans solution to a simpler analytical form and extended its use to different geometries. In this paper, a variation based on the Halpin–Tsai bounds will be used. This variation was developed and used by Odegard (2004)

$$\boldsymbol{E}_{il}^{*} = \boldsymbol{E}_{il}^{M}\frac{1 + \sum_{r=2}^{N}\eta_{il}^{r}c^{r}}{1 - \sum_{r=2}^{N}\eta_{il}^{r}c^{r}} \tag{18}$$

where

$$\eta_{il}^{r} = \frac{\boldsymbol{E}_{il}^{I,r} - \boldsymbol{E}_{il}^{M}}{\boldsymbol{E}_{il}^{I,r} + \boldsymbol{E}_{il}^{M}} \tag{19}$$

3.6. Hashin–Shtrikman bounds

The approach of Hashin and Shtrikman (1963) calculates the tightest bounds possible for a two-phase material, andis based on the Mori–Tanaka method. The approach leads to upper and lower bounds, which can be calculated by applying the Mori–Tanaka method considering the matrix material to have the best properties for the upper bound, and interchanging phases for the lower bound. In our case, the piezoelectric material is stiffer than the air contained in the porous inclusions. Hence, it is used as matrix material to obtain the lower bound. Thus

$$\boldsymbol{E}_{(HS+)}^{*} = \boldsymbol{E}^{I} + c^{M}\left[\left(\boldsymbol{E}^{M} - \boldsymbol{E}^{I}\right)^{-1} + c^{I}\boldsymbol{S}^{I}\left(\boldsymbol{E}^{I}\right)^{-1}\right]^{-1} \quad \text{and}$$

$$\boldsymbol{E}_{(HS-)}^{*} = \boldsymbol{E}^{M} + c^{I}\left[\left(\boldsymbol{E}^{I} - \boldsymbol{E}^{M}\right)^{-1} + c^{M}\boldsymbol{S}^{M}\left(\boldsymbol{E}^{M}\right)^{-1}\right]^{-1} \tag{20}$$

The upper Hashin–Shtrikman bound should be calculated with care, since it requires the inverse of the inclusion electroelastic material matrix, which in our case (air) is assumed to be singular. Since the stiffness of the air inclusion is negligible, the upper bound defined in Eq. (20) ($\boldsymbol{E}_{(HS+)}^{*}$) tends to zero in the resultant electromechanical stiffness matrix. However, the lower bound ($\boldsymbol{E}_{(HS-)}^{*}$) represents the maximum values. Thus the bounds are inverted, although the definitions used in this paper are not changed, in order to be consistent with the literature.

4. Finite elements modelling of the RVE

4.1. Representative volume element (RVE).

To apply the Finite Element Method (FEM), we need to define the dimensions and characteristics of the model or the part of the model we are going to simulate. As highlighted in Section 3.1 the representative volume should be statistically representative of the macro-element. This can be done by choosing a correct size of RVE, which normally is a cube with a specific side length L_{RVE}. The effective properties of the material are obtained by volume averaging (or homogenization) on a "computational cell" with typical size. For a random micro-structure, the true effective properties are obtained as the converged values when L_{RVE} becomes sufficiently large. However, in practice, to avoid excessive computational costs, it is necessary to choose a cell of finite size.

For the non-random case considered here, a cell size is used that represents the smallest periodic geometry which is still representative of the material configuration. In the case of complete scale separation, in order to quantify as an RVE, the size L_{RVE} must be:

- sufficiently small compared to the typical macro-scale dimension of the structural component.
- sufficiently large compared to the typical sub-scale dimension of constituents.

That the RVE is sufficiently small means that the averaged field variables, e.g. stress and strains, vary at most linearly within the RVE, as seen in Section 3.1. That the RVE is sufficiently large means that the averaged field variables for a given macroscopic "point" do not change significantly with a further increase of the RVE size. Nemat-Nasser and Hori (1993) discussed the size of the RVE in more detail. Obviously, the RVE size will be conditioned by the size of the inclusions. The porous regions or inclusions are air spheres whose diameter depends on the fabrication method. For polymers made using self-raising flour, the diameters are between 30–90 μm (Bowen et al., 2004). When the BurPS process is chosen, which burns out polymer spheres when the mix is exposed to high temperatures, the diameters are between 70–200 μm (Bowen et al., 2004). In some cases, for example when poly(methyl methacrylate) is used, the diameters can be over the 200 μm. These processes are detailed in Section 4.3. Knowing the distribution of the inclusions inside the matrix and their size, we can choose an appropriate RVE size. The distribution of inclusions in the RVE in the numerical model developed in this paper corresponds to a homogeneous and perfect distribution which allows us to establish a fair comparison with the analytical models which do not consider random distributions of inclusions. The computational cost is also reduced significantly by only considering a single inclusion geometry.

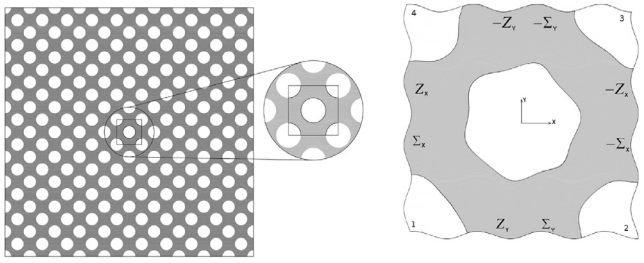

(a) Periodicity: RVE inside an infinite matrix of RVEs.

(b) Periodic boundary conditions definition

Fig. 1. Periodic boundary conditions for a representative volume element.

If the RVE is statistically representative of the composite geometry and properties, then $\overline{\boldsymbol{E}} = \overline{\boldsymbol{F}}^{-1}$ as seen in Eq. (6). A consistent averaging technique is expected to satisfy this inverse relation.

4.2. Periodic boundary conditions

A numerical model is simulated to compare with the analytical results, using a finite element model, based on the simulated RVE. These elements have properties corresponding to the phase they are contained within. The definition of the element properties is straightforward as soon as we know the properties of the phases (PZT and air) and the geometrical distribution. To define completely a numerical model, appropriate boundary conditions have to be defined. These boundary conditions have to represent the behaviour of the heterogeneous material RVE in a specific situation, for example in a traction test (Dirichlet conditions or Neumann conditions) or inside a matrix of a repeated RVE (Periodic Boundary Conditions). Periodic boundary conditions can be formulated for unit cells when the volume exhibits a periodic structure. Terada et al. (2000) investigated the application of periodic boundary conditions in micromechanics. He showed that:

- Periodic boundary conditions applied on a relative small RVE provides reasonable estimates of the effective properties even if the medium doesn't have actual periodicity.
- Periodic boundary conditions give a more reasonable estimate of the effective moduli than either Dirichlet or Neumann boundary conditions.

As shown in Fig. 1b, the chosen boundary conditions imply that the opposite edges have identical deformation, and opposite stress direction (Suquet, 1985). These conditions simulate the boundary conditions created by an infinite matrix surrounding the RVE, as shown in Fig. 1a. This matrix is supposed to consist of an infinite series of RVEs repeating in all directions. This assumptions allows us to choose the minimum RVE which ensures a representative geometry, and hence to the model a single simple inclusion geometry.

To simulate the periodic boundary conditions in ANSYS®, a macro links all boundary nodal displacements depending on their position. To link correctly the values of the displacements between opposite nodes, the relative position of this node with respect to their surface has to be the same. This means that the meshes should be equal on the opposite faces. To achieve this, we mesh the primary surfaces and copy this mesh to the secondary surfaces. When all surfaces are generated, we generate the volume mesh. Berger et al. (2005) used only one element in the transverse direction due to the transverse isotropic behaviour, but here we consider the volume is a 3D cubic volume with sides equal to L. Also each node has only three mechanical (displacements in X, Y and Z directions) and one electrical (voltage VOLT) degrees of freedom, and so appropriate relative displacements between surfaces in the correct directions have to be used to simulate the tangential stresses.

In this paper, periodic boundary conditions are applied to a periodic porous structure consisting of a piezoelectric material matrix and air inclusions in different percentages.

4.3. Finite element model

To model the representative volume of our porous piezoelectrical material, first we need to define the materials that will be used. Formed by two phases, the RVE is made of air and a piezoelectrical material. The air phase will be meshed and modelled as a material with low elastic properties, about 100 N/m^2 which is small compared to the piezoelectric elastic properties, which has order 10^{10} N/m^2. The relative permittivity of the air is defined as 1.

The air parts are meshed in order to fulfil the requirements of Eq. (9) which means the values measured have to be averaged over all regions of the RVE. Furthermore, not all of the properties of air are zero, for example the permittivity will be non-zero. Thus, by meshing the air, a general purpose framework for computational optimization can be built, and this decreases the possibilities of numerical issues arising from the use of zero elastic properties in the FEM model. The piezoelectrical material chosen is the synthetic ceramic PZT-5A, which is one of the most used in engineering. The properties of this material are given by Erturk and Inman (2011). The PZT-5A is a transverse isotropic material and its properties are given in Eq. (21), with units given in Eq. (22).

$$\boldsymbol{E}^M = \left(\begin{array}{cccccc|ccc} 121 & 75.4 & 75.2 & 0 & 0 & 0 & 0 & 0 & 5.4 \\ & 121 & 75.2 & 0 & 0 & 0 & 0 & 0 & 5.4 \\ & & 111 & 0 & 0 & 0 & 0 & 0 & -15.8 \\ & & & 21.1 & 0 & 0 & 0 & -12.3 & 0 \\ & \multicolumn{2}{c}{\textit{Symmetric}} & & 21.1 & 0 & -12.3 & 0 & 0 \\ & & & & & 22.9 & 0 & 0 & 0 \\ \hline 0 & 0 & 0 & 0 & 12.3 & & 919 & 0 & 0 \\ 0 & 0 & 0 & 12.3 & 0 & 0 & & 919 & 0 \\ -5.4 & -5.4 & 15.8 & 0 & 0 & 0 & \multicolumn{3}{c}{\textit{Symm.}} & 826.6 \end{array}\right) \tag{21}$$

$$\text{Units} = \left(\begin{array}{c|c} C\ (\text{GPa}) & e^T\ (\text{C/m}^2) \\ \hline e\ (\text{C/m}^2) & k_T/k_0 \end{array}\right) \qquad k_0 = 8.854 \times 10^{-12}\text{pF/m} \tag{22}$$

Once the material properties of the different phases are defined, the next step is to model the geometry of the volume. The geometry is composed of two spheres in a matrix, one in the center, the other distributed equally in the corners of the RVE. We should note that imperfections in the sphere shapes are possible as a result of the fabrication process. There are two main processes to generate porosity in a piezoelectric matrix. The most flexible in terms of the range of materials, and hence the most general, is the BurPS process. The name is derived from the process itself, "Burn out Polymer Sphere". In this process, the piezoelectric phase is fabricated as a powder or by ball milling and the most common materials are polyethylene oxide (PEO) and poly(methyl methacrylate) (PMMA) (Bowen et al., 2004). This mix is subjected to pressure equal to 50 MPa. At the same time, a heat treatment at 400 °C is used to burn off the volatile additive, and then the temperature is increased up to 1125 °C for 2 h to sinter the ceramic (Bowen et al., 2004). This technique is limited to percentages of inclusion lower than 70% (Kara et al., 2003). Using the BurPS process, the overlapping of inclusions is minimum, reduced only to spheres "touching" each other, because the polymer spheres cannot overlap each other. The shape of the inclusions is consistent, because the spheres maintain their shape during the process of the increasing heat until they disappear. Also an elaborate and careful fabrication process can lead to a relatively homogeneous and regular distribution. Some authors have studied the influence of the shape of inclusions in the piezoelectric material properties using assumptions such as cuboidal porosity (Bosse et al., 2012). The authors also conclude that "the fundamental elastic, piezoelectric and dielectric constants increase nonlinearly with the increase in material volume fraction."

The second most common process to manufacture porous piezoelectric materials is the self-raising method. In this process, the final inclusion size is finer than in the BurPS case. In this process the porous inclusion are grown from inside of the matrix. The deformation of the inclusion and overlapping are both likely because the bubbles of air created in the process intersect and connect to each other, changing their size and shape.

In our model, we suppose the test is prepared using a BurPS process, so the possible deformation of the inclusions and the overlapping of particles are neglected. Also a regular distribution of the inclusions in the matrix is considered. Although clearly unrealistic, this configuration should show the best possible results avoiding conglomeration effects, shape deformations and particles overlapping. The comparison with the analytical theories is then more fair.

The geometry of the model is then defined by an inclusion in the center of the RVE and a segment of an inclusion in each corner, as shown in Fig. 2. The size of the RVE is chosen to reduce computational cost but is still representative of the geometry of the material.

In the finite element model one of the most important steps in the setup process is to configure the boundary conditions, and periodic boundary conditions will be used here. In terms of the modelling, this means that each node (i) has its displacements related with those of node (j) on the opposite surface. These displacements are related through the strain applied in the model as Berger et al. (2005) explained. Thus

$$U_M^j - U_M^i = Z_{Mn}(x_n^j - x_n^i) \Rightarrow \begin{cases} u_m^j - u_m^j & = \epsilon_{mn}(x_n^j - x_n^i) \\ \phi^j - \phi^i & = E_n(x_n^j - x_n^i) \end{cases}$$

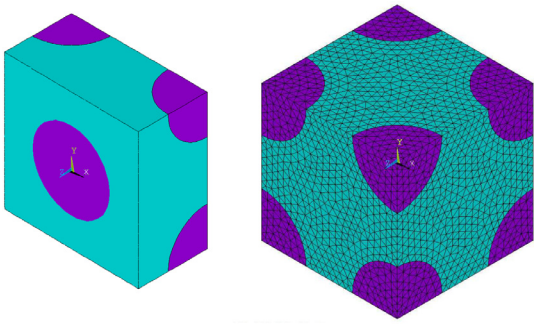

(a) Inner inclusion view (b) Mesh Element view

Fig. 2. Different views of the representative volume element.

To avoid rigid body motion, the displacements and voltage of one of the points are fixed to zero. In our case, the point (0, 0, $R_{inclusion}$).

The geometry is programmed into the FEM program ANSYS® using its programming language APDL. A script with all of the geometry and boundary conditions was written as a function of the displacement applied and the percentage of inclusion.

4.4. Evaluation of the different effective coefficients

The boundary conditions are applied and the results are obtained using ANSYS® integrated solver, namely the stress and strain for each element and node. The macro parameters are obtained through the volumetric mean using Eq. (9). These equations will be approximated by the weighted average over the RVE volume as

$$\overline{\boldsymbol{\sigma}} = \frac{1}{V}\sum_V \boldsymbol{\sigma_e}\, V_e, \quad \overline{\boldsymbol{\epsilon}} = \frac{1}{V}\sum_V \boldsymbol{\epsilon_e}\, V_e,$$
$$\overline{\boldsymbol{D}} = \frac{1}{V}\sum_V \boldsymbol{D_e}\, V_e, \quad \overline{\boldsymbol{E}} = \frac{1}{V}\sum_V \boldsymbol{E_e}\, V_e \tag{23}$$

where the subindex "*e*" means the element number. From the volumetric mean of the parameters, the material parameters of the homogenized material are calculated from Eq. (7).

To obtain the 81 parameters which appear in Eq. (7) and constitute the electroelastic material properties matrix, we need at least 81 equations. Each test realised (one strain/electric field applied) generates 9 equations, derived from the nine elements of the strain/electric field vector. So, we should realise 9 different tests applying different strain/electric fields. We notice that the piezoelectric material is transverse isotropic and the air can be considered homogeneous, so that the composite material will have the higher grade of anisotropy of its components, and hence the composite will be transverse isotropic too. To define a transverse isotropic electroelastic matrix we do not need all 81 parameters, because some components are zero and additionally the elastic part is symmetric and the eletromechanical coupling coefficients of the main diagonal have opposite signs. Thus only 10 parameters are needed to define a transverse isotropic material: 5 mechanical, 3 piezoelectric and 2 dielectric. This reduces the number of tests to only 2, but it is preferred to realise the whole set to estimate the whole material matrix and check convergence, symmetry and possible errors introduced.

Having obtained the results for the nine tests, we proceed to solve the system of equations. Due to the periodic boundary conditions that relate the deformations in opposite sides, the expected deformation averaged volume values will be very small, except the displacement/electrical field applied as part of the characterization test. Hence the material parameters can be obtained from the relation

$$E_{nm} = \frac{\Sigma_n}{Z_m} \quad \text{for } n, m \in [1, 9]$$

where the subindex m corresponds to the strain/electric field applied and the n corresponds to the stress/electrical displacement response.

5. Results and comparison

The results obtained from the analytical and numerical models are shown in Figs. 3 and 4. Fig. 3 shows the five mechanical coefficients necessary to define a transverse isotropic material. In our case, the analytical theories are used for extreme cases as electromechanical homogenization and very different phases (air-PZT) but they show a good agreement between the mechanical coefficients with the numerical results. The Mori-Tanaka approach is one of the most advanced and reliable methods for analytical homogenization, and for this porous case shows a good match with the numerical results. This agreement holds for the whole range of inclusion percentage. For the mechanical coefficients, the self-consistent scheme also shows good agreement with the Mori-Tanaka and the numerical results, which it is expected due to the similar assumptions in both analytical methods and numerical methods, based on the averaging technique (*Mean field homogenization theory* and *Hill–Mandel condition*). The Hashin–Shtrikman bound offers results similar to the Halpin–Tsai bound, and for most of the mechanical parameters is an upper bound for the analytical results. For the piezoelectric coefficients, these bounds represent average values of the numerical results, which tends to give the highest values, and the analytical methods (Mori-Tanaka and Self-Consistent) which tends to underestimate these coefficients. The upper Hashin–Shtrikman bound cannot be calculated as explained in Section 3.6. The method proposed by Odegard (2004) is a geometrical approximation to the Halpin–Tsai bounds which is extended for the piezoelectric material. Hence the results are quite uniform in all graphs, and are in the middle of the results of the other methods.

Fig. 4 shows the piezoelectric and dielectric parameter results. There are larger differences between the analytical models and the numerical results. This is due to the nature of the model which has been extended from the mechanical part to the electric field. This leads to considerable differences between the different methods and an important variation of the results with respect to the numerical methods. In contrast, the dielectric coefficients show a better match between all theories and the numerical results. The Mori–Tanaka method shows the best agreement with the numerical results again.

For the piezoelectrical parameter results presented in Fig. 4, each method will be discussed in turn. The Mori–Tanaka method shows the best agreement with the numerical results for the coefficient e_{31}, which is the most dominant coefficient in energy harvesting applications. For the other coefficients, the differences are bigger and it underestimates the numerical values. The self-consistent method shows interesting results in the coefficient e_{31} where it shows an increase of the absolute value until 20% of inclusions and decreases after that but at lower ratio than the other methods. These results are very different from the numerical results. This increase in e_{31} for small percentages of inclusions might be due to the decrease in the permittivity coefficients and the very small increase in the strain in the matrix material for small percentage of inclusions. As stated before, the e_{31} coefficient is a ratio between the voltage measured, which is increased by the decreased permittivity, and the strain measured, which for small increases in inclusion percentage could be very small. For the other piezoelectric coefficients the agreement is better, and similar to the Mori-Tanaka approach. It is interesting to notice that

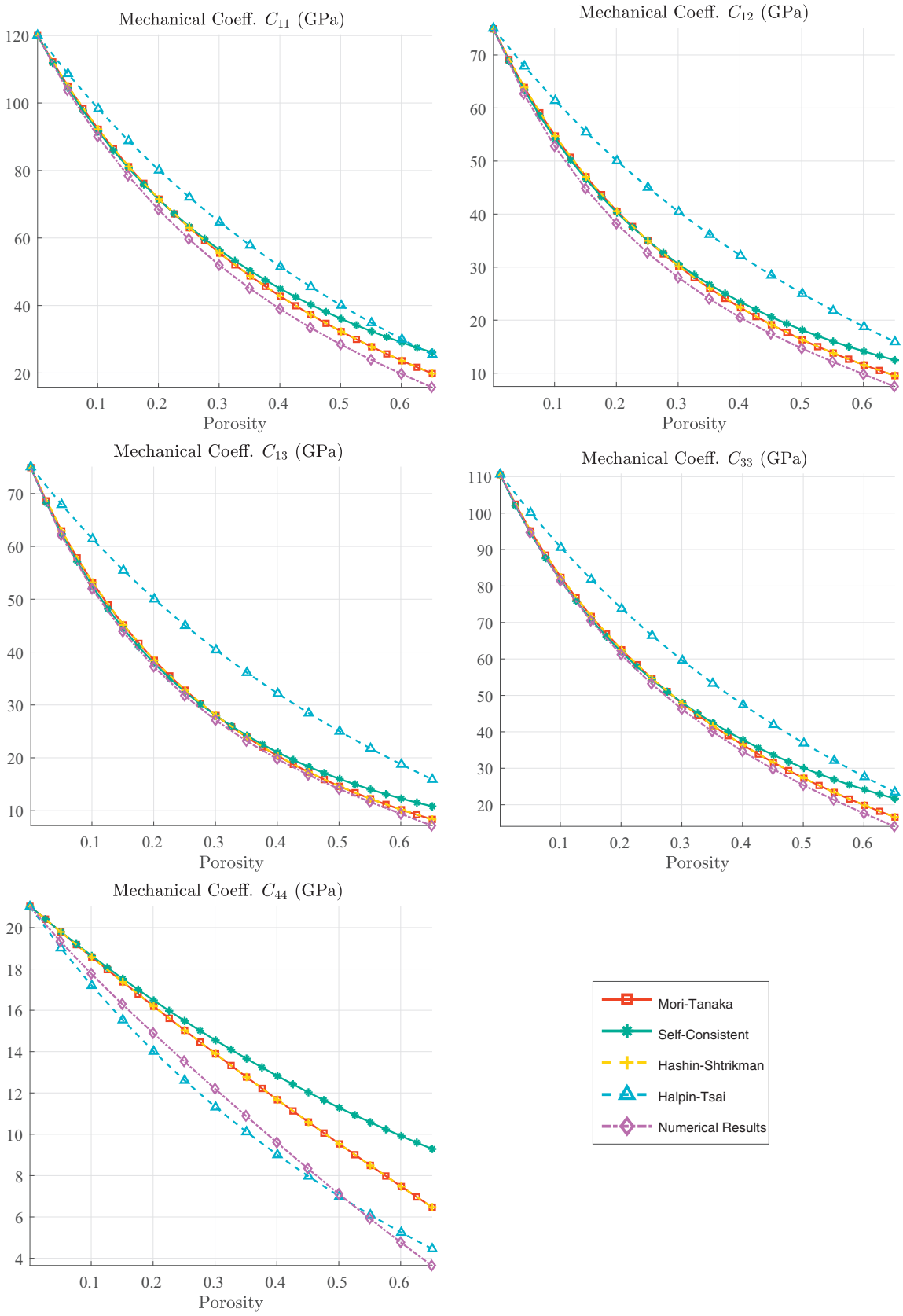

Fig. 3. The estimated mechanical coefficients.

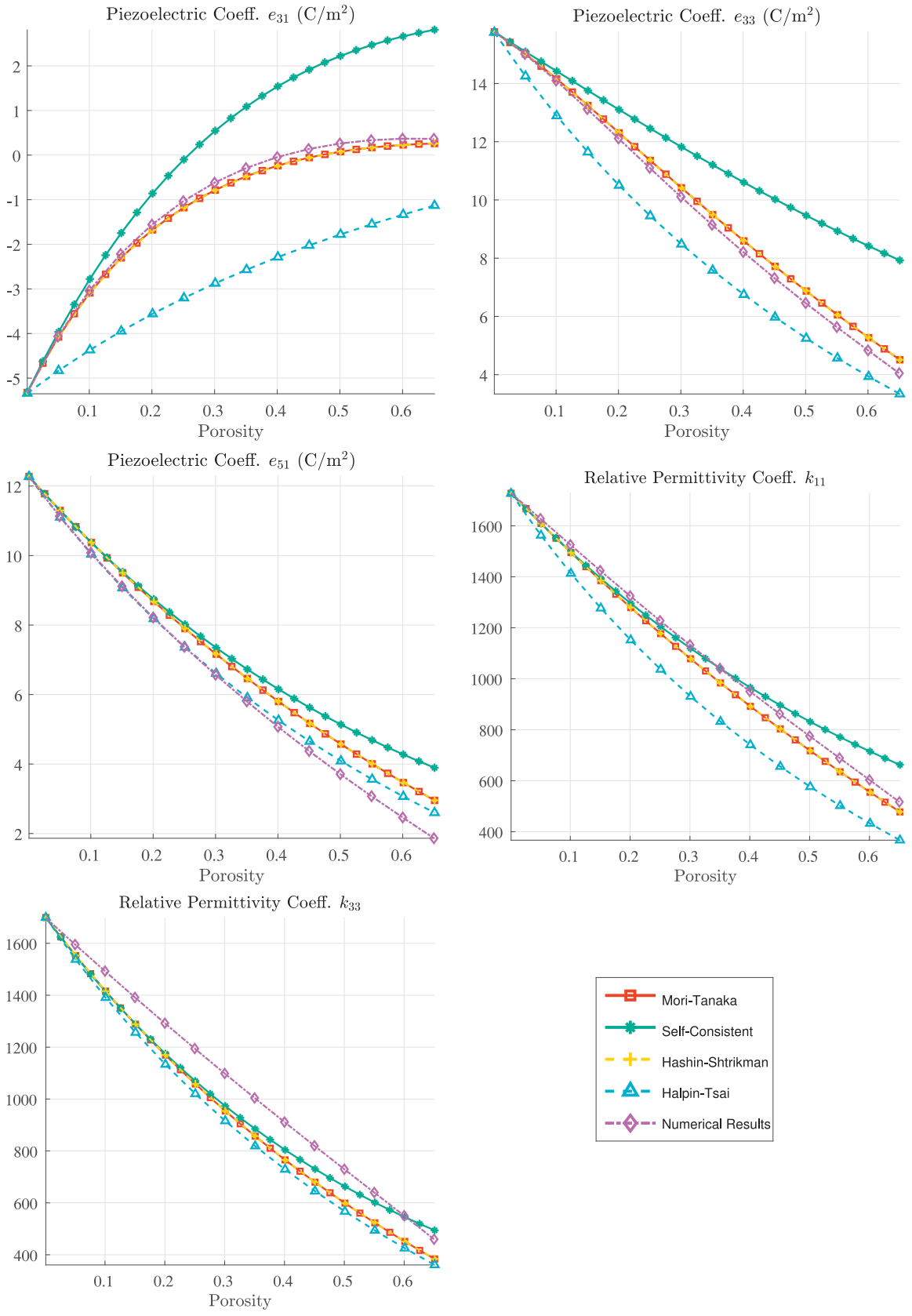

Fig. 4. The estimated piezoelectric and dielectric coefficients.

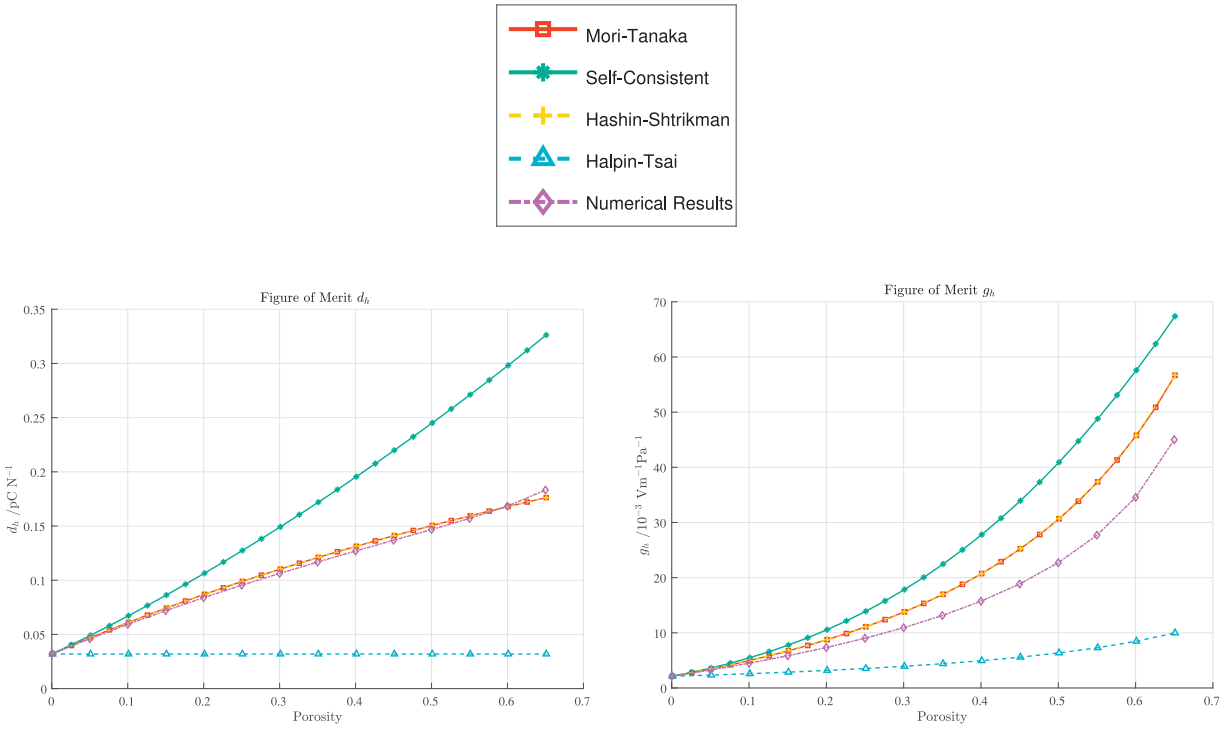

Fig. 5. The figures of merit d_h and g_h for the analytical and numerical methods.

the self-consistent results tend to overestimate the absolute value of the parameters for percentages of inclusions over 40–50%. The Halpin–Tsai method shows the same tendency as the mechanical coefficient results. Due to the geometrical variation, this method shows smooth and similar results for all coefficients. In the case of the Hashin–Shtrikman bounds the results are between the self-consistent method and the numerical results, and are best for the capacitative coefficient which is plotted as relative permittivity k_{33}.

It is interesting to notice the linearity of the numerical results with respect to the percentage of inclusions. In the case of the mechanical coefficients, this linearity is not so clear. This linearity arises from the small impact of the electromechanical coupling with respect to the impact of the inclusion percentage, as this percentage is the main driver for the change in these parameters. The same logic can be applied to the dielectric coefficients, which again show the dominance of the percentage inclusions over any other coupling.

These results can be used to obtain the figures of merit of the porous piezoelectric material. These figures are relationships between material coefficients which express the potential amount of energy the material can generate independently of the geometry, excitation or electrical connection. Higher values of these coefficients represent higher capability to generate energy. As a comparison, the coefficients d_h and g_h are presented. These coefficients are defined as

$$d_h = d_{33} + 2 \cdot d_{31} \tag{24}$$

$$g_h = \frac{d_h}{k_{\sigma,33}} \tag{25}$$

The coefficients d are the piezoelectric coefficients expressed when the dependent variables are the strains (ϵ) and the electrical displacement (D). This is also called the strain-charge form.

$$\begin{aligned} \epsilon &= S_E \cdot \sigma + d^T \cdot E \\ D &= d \cdot \sigma + k_\sigma \cdot E \end{aligned} \tag{26}$$

where the subindex σ and E in k_σ and S_E mean the permittivity and stiffness are measured under constant stress σ and electrical field E respectively. When T appears as superindex, it means transpose of the matrix. In the present paper, the stress-charge form has been used (see eq. 1), where the dependent variables are the stresses σ and the electrical displacement D. Hence the appropriate change is necessary using the relationships:

$$\begin{aligned} S_E &= C_E^{-1} \\ d &= e\, S_E \\ k_\sigma &= k_\epsilon + d \cdot C_E^{-1} \cdot d^T \end{aligned} \tag{27}$$

The coefficient d_h represents the total amount of energy generated by the piezoelectric effect, and the g_h represents the energy output when the losses due to the permittivity are included.

In Fig. 5 the evolution of these coefficients with respect to the porosity is presented. These coefficients increase for higher porosity, specially the coefficient g_h which increases rapidly for porosity percentages higher than 20%. The coefficient d_h does not show much variability with respect to the porosity, with changes smaller than 1% compared to the strain coefficients d. In contrast, the coefficient g_h increases as a consequence of the small decreases in the piezoelectric coefficients, represented by d_h, and the important decrease in the permittivity e_{33} (see Fig. 4). Thus the porous piezoelectric materials show improved properties for energy harvesting compared to dense piezoelectric materials. This conclusion agrees with the results presented by Bowen et al. (2004). In this study the coefficient d_h remains relatively constant for porosity percentages up to 50% where the PZT structure is compromised due to the high level of porosity. Furthermore, the coefficient g_h shows a significant increase compared to the non-porous material, as Bowen et al., 2004 reported. Hence the approach presented in this paper appears to be valid for porosity up to 50%.

6. Conclusions

A new approach to the homogenization of porous piezoelectric materials has been given. Using different analytical methods developed in this paper, a comparison between these results and their corresponding finite element estimates is performed. From the comparison of both approaches the following conclusions can be drawn:

- The analytical models are well-developed for the elastic homogenization of composite material, with only small differences to the numerical methods, independent of the nature of the constituent of the composite.
- The same methods give good estimates of the piezoelectric properties for small percentages of inclusions. Especially for the piezoelectric coefficient e_{31} the Mori–Tanaka method gives good estimates of the composite coefficients, making this analytical approach suitable for energy harvester design.
- Although the analytical and numerical methods show reasonable agreement in the dielectric parameters, these parameters show some errors due to their order which is much more smaller than the other values in the electroelastic material matrix.
- Porous piezoelectric materials present important advantages for energy harvesting compared to dense piezoelectric materials as a consequence of the beneficial ratio between the piezoelectric coefficients and the permittivity when the porosity is increased.

Acknowledgment

The authors acknowledge the financial support from the Sêr Cymru National Research Network and Swansea University through a Postgraduate Scholarship.

References

Adhikari, S., Friswell, M.I., Inman, D.J., 2009. Piezoelectric energy harvesting from broadband random vibrations. Smart Mater. Struct. 18 (11), 115005.
Anton, S.R., Sodano, H.A., 2007. A review of power harvesting using piezoelectric materials (2003–2006). Smart Mater. Struct. 16 (3), R1.
Balzani, D., Scheunemann, L., Brands, D., Schröder, J., 2014. Construction of two-and three-dimensional statistically similar RVEs for coupled micro-macro simulations. Comput. Mech. 54 (5), 1269–1284.
Barnett, D.M., Lothe, J., 1975. Dislocations and line charges in anisotropic piezoelectric insulators. Physica Status Solidi (b) 67 (1), 105–111.
Beeby, S.P., Tudor, M.J., White, N.M., 2006. Energy harvesting vibration sources for microsystems applications. Meas. Sci. Technol. 17 (12), R175.
Benveniste, Y., 1987. A new approach to the application of Mori–Tanaka's theory in composite materials. Mech. Mater. 6 (2), 147–157.
Berger, H., Kari, S., Gabbert, U., Rodriguez-Ramos, R., Guinovart, R., Otero, J.A., Bravo–Castillero, J., 2005. An analytical and numerical approach for calculating effective material coefficients of piezoelectric fiber composites. Int. J. Solids Struct. 42 (21), 5692–5714.
Bosse, P.W., Challagulla, K.S., Venkatesh, T., 2012. Effects of foam shape and porosity aspect ratio on the electromechanical properties of 3-3 piezoelectric foams. Acta Mater 60 (19), 6464–6475.
Boucher, S., 1974. On the effective moduli of isotropic two-phase elastic composites. J. Compos. Mater. 8 (1), 82–89.
Bowen, C.R., Perry, A., Lewis, A.C.F., Kara, H., 2004. Processing and properties of porous piezoelectric materials with high hydrostatic figures of merit. J. Eur. Ceram. Soc. 24 (2), 541–545.
Cook-Chennault, K.A., Thambi, N., Sastry, A.M., 2008. Powering mems portable devices: a review of non-regenerative and regenerative power supply systems with special emphasis on piezoelectric energy harvesting systems. Smart Mater. Struct. 17 (4), 043001.
Deeg, W.F.J., 1980. The analysis of dislocation, crack, and inclusion problems in piezoelectric solids.
Dunn, M.L., Taya, M., 1993. An analysis of piezoelectric composite materials containing ellipsoidal inhomogeneities. In: Proceedings of the Royal Society of London A: Mathematical, Physical and Engineering Sciences, 443. The Royal Society, pp. 265–287.
Dunn, M.L., Taya, M., 1993. Electromechanical properties of porous piezoelectric ceramics. J. Am. Ceram. Soc. 76 (7), 1697–1706.
Dunn, M.L., Taya, M., 1993. Micromechanics predictions of the effective electroelastic moduli of piezoelectric composites. Int. J. Solids Struct. 30 (2), 161–175.
Erturk, A., Inman, D.J., 2008. On mechanical modeling of cantilevered piezoelectric vibration energy harvesters. J. Intell. Mater. Syst. Struct.
Erturk, A., Inman, D.J., 2009. An experimentally validated bimorph cantilever model for piezoelectric energy harvesting from base excitations. Smart Mater. Struct. 18 (2), 025009.
Erturk, A., Inman, D.J., 2011. Piezoelectric Energy Harvesting. John Wiley & Sons.
Eshelby, J.D., 1957. The determination of the elastic field of an ellipsoidal inclusion, and related problems. In: Proceedings of the Royal Society of London A: Mathematical, Physical and Engineering Sciences, 241. The Royal Society, pp. 376–396.
Feyel, F., 2003. A multilevel finite element method (fe 2) to describe the response of highly non-linear structures using generalized continua. Comput. Methods Appl. Mech. Eng. 192 (28), 3233–3244.
Fish, J., Shek, K., Pandheeradi, M., Shephard, M.S., 1997. Computational plasticity for composite structures based on mathematical homogenization: theory and practice. Comput. Methods Appl. Mech. Eng. 148 (1–2), 53–73.
Friswell, M.I., Ali, S.F., Bilgen, O., Adhikari, S., Lees, A.W., Litak, G., 2012. Non-linear piezoelectric vibration energy harvesting from a vertical cantilever beam with tip mass. J. Intell. Mater. Syst. Struct. 23 (13), 1505–1521.
Geers, M.G., Kouznetsova, V., Brekelmans, W., 2001. Gradient-enhanced computational homogenization for the micro-macro scale transition. Le Journal de Physique IV 11 (PR5), Pr5–145.
Geers, M.G., Kouznetsova, V., Brekelmans, W., 2010. Multi-scale computational homogenization: trends and challenges. J. Comput. Appl. Math. 234 (7), 2175–2182.
Gururaja, T.R., Schulze, W.A., Cross, L.E., Newnham, R.E., Auld, B.A., Wang, Y.J., et al., 1985. Piezoelectric composite materials for ultrasonic transducer applications. part i: resonant modes of vibration of pzt rod-polymer composites. IEEE Trans. Sonics Ultrason 32 (19985), 481–498.
Hashin, Z., Shtrikman, S., 1963. A variational approach to the theory of the elastic behaviour of multiphase materials. J. Mech. Phys. Solids 11 (2), 127–140.
Hermans, J.J., 1967. Koninklijke Nederlandse Akademie van Wetenschappen, Amsterdam. Proc. Ser. B 70, 1.
Hershey, A.V., 1954. The elasticity of an isotropic aggregate of anisotropic cubic crystals. J. Appl. Mech.-Trans. ASME 21 (3), 236–240.
Hill, R., 1963. Elastic properties of reinforced solids: some theoretical principles. J. Mech. Phys. Solids 11 (5), 357–372.
Hill, R., 1965. A self-consistent mechanics of composite materials. J. Mech. Phys. Solids 13 (4), 213–222.
Kar-Gupta, R., Venkatesh, T.A., 2007. Electromechanical response of porous piezoelectric materials: effects of porosity distribution. Appl. Phys. Lett. 91 (6), 062904.
Kara, H., Ramesh, R., Stevens, R., Bowen, C.R., 2003. Porous pzt ceramics for receiving transducers. Ultrasonics, Ferroelectrics, and Frequency Control, IEEE Transactions on 50 (3), 289–296.
Klusemann, B., Böhm, H.J., Svendsen, B., 2012. Homogenization methods for multi--phase elastic composites with non-elliptical reinforcements: comparisons and benchmarks. Eur. J. Mech.-A/Solids 34, 21–37.
Klusemann, B., Svendsen, B., 2010. Homogenization methods for multi-phase elastic composites: comparisons and benchmarks. Technische Mechanik 30 (4), 374–386.
Kouznetsova, V., Geers, M., Brekelmans, W., 2004. Multi-scale second-order computational homogenization of multi-phase materials: a nested finite element solution strategy. Comput. Methods Appl. Mech. Eng. 193 (48), 5525–5550.
Kröner, E., 1958. Berechnung der elastischen konstanten des vielkristalls aus den konstanten des einkristalls. Zeitschrift für Physik 151 (4), 504–518.
Kurukuri, S., Eckardt, S., 2004. A review of homogenization techniques for heterogeneous materials. Advanced Mechanics of Materials and Structures. Graduate School in Structural Engineering, Germany.
Li, J.-F., Takagi, K., Ono, M., Pan, W., Watanabe, R., Almajid, A., Taya, M., 2003. Fabrication and evaluation of porous piezoelectric ceramics and porosity–graded piezoelectric actuators. J. Am. Ceram. Soc. 86 (7), 1094–1098.
Miehe, C., Schröder, J., Becker, M., 2002. Computational homogenization analysis in finite elasticity: material and structural instabilities on the micro-and macro-scales of periodic composites and their interaction. Comput. Methods Appl. Mech. Eng. 191 (44), 4971–5005.
Miehe, C., Schröder, J., Schotte, J., 1999. Computational homogenization analysis in finite plasticity simulation of texture development in polycrystalline materials. Comput. Methods Appl. Mech. Eng. 171 (3–4), 387–418.
Mikata, Y., 2000. Determination of piezoelectric eshelby tensor in transversely isotropic piezoelectric solids. Int. J. Eng. Sci. 38 (6), 605–641.
Mishnaevsky Jr, L.L., 2007. Computational Mesomechanics of Composites: Numerical Analysis of the Effect of Microstructures of Composites of Strength and Damage Resistance. John Wiley & Sons.
Moës, N., Cloirec, M., Cartraud, P., Remacle, J.F., 2003. A computational approach to handle complex microstructure geometries. Comput. Methods Appl. Mech. Eng. 192 (28), 3163–3177.
Mori, T., Tanaka, K., 1973. Average stress in matrix and average elastic energy of materials with misfitting inclusions. Acta Metall. 21 (5), 571–574.
Nemat-Nasser, S., Hori, M., 1993. Micromechanics: Overall properties of heterogeneous materials. Elsevier.
Nemat-Nasser, S., Yu, N., Hori, M., 1993. Bounds and estimates of overall moduli of composites with periodic microstructure. Mech. Mater. 15 (3), 163–181.
Newnham, R.E., 1986. Composite electroceramics. Ferroelectrics 68 (1), 1–32.
Norris, A.N., 1985. A differential scheme for the effective moduli of composites. Mech. Mater. 4 (1), 1–16.

Odegard, G.M., 2004. Constitutive modeling of piezoelectric polymer composites. Acta Mater. 52 (18), 5315–5330.
Pierard, O., Friebel, C., Doghri, I., 2004. Mean-field homogenization of multi-phase thermo-elastic composites: a general framework and its validation. Compos. Sci. Technol. 64 (10), 1587–1603.
Roncari, E., Galassi, C., Craciun, F., Capiani, C., Piancastelli, A., 2001. A microstructural study of porous piezoelectric ceramics obtained by different methods. J. Eur. Ceram Soc. 21 (3), 409–417.
Roscow, J., Zhang, Y., Taylor, J., Bowen, C.R., 2015. Porous ferroelectrics for energy harvesting applications. Eur. Phys. J. Special Topics 224 (14–15), 2949–2966. doi:10.1140/epjst/e2015-02600-y.
Schröder, J., Balzani, D., Brands, D., 2011. Approximation of random microstructures by periodic statistically similar representative volume elements based on lineal-path functions. Arch. Appl. Mech. 81 (7), 975–997.
Sodano, H.A., Inman, D.J., Park, G., 2004. A review of power harvesting from vibration using piezoelectric materials. Shock Vibr. Digest 36 (3), 197–206.
Sodano, H.A., Inman, D.J., Park, G., 2005. Comparison of piezoelectric energy harvesting devices for recharging batteries. J. Intell. Mater. Syst. Struct. 16 (10), 799–807.
Suquet, P.M., 1985. Local and global aspects in the mathematical theory of plasticity. Plast. Today 279–310.
Terada, K., Hori, M., Kyoya, T., Kikuchi, N., 2000. Simulation of the multi-scale convergence in computational homogenization approaches. Int. J. Solids Struct. 37 (16), 2285–2311.
Vijaya, M.S., 2012. Piezoelectric materials and devices: applications in engineering and medical sciences. CRC Press.
Wu, T.T., 1966. The effect of inclusion shape on the elastic moduli of a two-phase material. Int. J. Solids Struct. 2 (1), 1–8.
Zou, W., He, Q., Huang, M., Zheng, Q., 2010. Eshelby's problem of non-elliptical inclusions. J. Mech. Phys. Solids 58 (3), 346–372.
Zouari, R., Benhamida, A., Dumontet, H., 2008. A micromechanical iterative approach for the behavior of polydispersed composites. Int. J. Solids Struct. 45 (11), 3139–3152.